Na@La-modified zeolite particles for simultaneous removal of ammonia nitrogen and phosphate from rejected water: performance and mechanism

Wenjiao Sang, Longjie Mei, Shiwen Hao, Dong Li, Xiaoyang Li, Qian Zhang, Xi Jin and Cuihua Li

ABSTRACT

Rejected water from sludge processing in wastewater treatment plants (WWTPs) is very harmful due to its high concentration of ammonia nitrogen and phosphorus. It is therefore necessary to find a low-cost and convenient technique to simultaneously remove ammonia nitrogen and phosphorus from rejected water. In this study, natural granular zeolite was modified by NaCl and $La(OH)_3$ to obtain a new material (Na@La-MZP), with several advantages compared with powdered zeolite. Na@La-MZP could remove 92.61% ammonia nitrogen (50 mg/L) and 99.01% phosphate (60 mg/L) at the optimal conditions of dosage 12.5 g/L, initial pH 6.0 and reaction time 12 hours, which enabled the effluent to satisfy the discharge standard (GB 18918-2002) for municipal WWTPs in China. The maximum adsorption capacity of Na@La-MZP was determined as 17.92 mg NH_4^+-N/g and 9.53 mg P/g by the Langmuir isotherm. Pseudo-second-order kinetics could well illustrate the adsorption process and show that the ammonia nitrogen and phosphate can be degraded by chemical reaction. The characterizations of Na@La-MZP confirmed the removal mechanism of ammonia nitrogen and phosphate. The Na@La-MZP still maintained more than 75% removal efficiency after five reuses. Furthermore, the estimated cost of this treatment method was 0.22 \$/m^3 rejected water.

Key words | high ammonia nitrogen, high phosphate, Na@La modified zeolite, rejected water, simultaneous removal

Wenjiao Sang (corresponding author)
Longjie Mei
Shiwen Hao
Dong Li
Qian Zhang
Xi Jin
Cuihua Li
School of Civil Engineering and Architecture,
Wuhan University of Technology,
Wuhan 430070,
China
E-mail: *whlgdxswj@126.com*

Xiaoyang Li
China Machinery International Engineering Design & Research Institute Company,
Limited, No. 18 Shaoshan Middle Road, Changsha 410007,
China

HIGHLIGHTS

- Na@La-MZP was used for simultaneous removal of NH_4^+-N and phosphate from rejected water.
- 92.61% NH_4^+-N and 99.01% phosphate were simultaneously removed by Na@La-MZP.
- Effluent satisfied the discharge standard for pollutants from municipal WWTPs.
- Removal efficiency of NH_4^+-N and phosphate remained above 75% after five cycles.
- Na@La-MZP showed excellent treatment of real rejected water.

doi: 10.2166/wst.2020.541

GRAPHICAL ABSTRACT

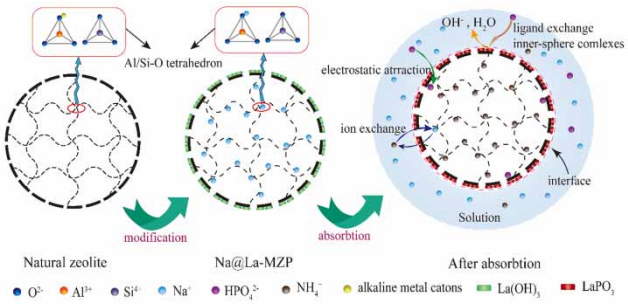

INTRODUCTION

Rejected water is a low C/N ratio, high ammonia nitrogen and phosphate wastewater produced in the process of excess sludge dewatering (Cheng *et al.* 2010). Presently, the traditional treatment method for rejected water is to transport it to the first wastewater tank in wastewater treatment plants (WWTPs) and mix it with the total influent of the process (Hu *et al.* 2015). Although it only accounts for about 5% of the wastewater processed by WWTPs, it can contribute 10–50% of the nitrogen load and 10–80% of the phosphorus load to the biochemical pond (Ivanov *et al.* 2009; Torà *et al.* 2014; Ren *et al.* 2015). If the treatment scale is small, there is a huge risk that the effluent quality will not satisfy the discharge standard of the WWTPs and even threaten their usual operation. In China, the production of rejected water was about 310 million m^3/d in 2020 (Hu *et al.* 2015; Ge *et al.* 2019). Hence, it is important to find a rejected water treatment technique to protect the water.

Presently, various wastewater treatment technologies have been developed to remove different pollutants, such as biological treatment, advanced oxidation technology, and adsorption (Zhang *et al.* 2016a, 2016b, 2016c; Kumari *et al.* 2020; Iqbal *et al.* 2021). Due to the advantages of simple processing technology and high efficiency, adsorption has attracted most attention (Iqbal *et al.* 2019; Pham *et al.* 2019; Song *et al.* 2020). The development and application of low-cost materials with high adsorption performance have been a focus of investigation. Until now, various materials have been widely used to remove ammonia nitrogen and phosphorus from wastewater, including biochar, bentonite, ion exchange resins, graphene, magnetic cationic hydrogel and zeolite (Copetti *et al.* 2016; Mazloomi & Jalali 2016; Zhang *et al.* 2016a, 2016b, 2016c; Dong *et al.* 2017; Xu *et al.* 2018).

Among them, natural zeolite is a three-dimensional framework composed of silicon, aluminum and oxygen (Motsi *et al.* 2009). The charge is unbalanced in the aluminum oxygen tetrahedron, therefore the natural zeolite surface is negatively charged (Jiang *et al.* 2018). To maintain charge equilibrium, alkaline earth metal cations are used to compensate around the tetrahedron. These metal cations can combine with the skeleton structure through weak bonds and flow effortlessly, so ion exchange reactions are easy with NH_4^+ in aqueous solutions (Montalvo *et al.* 2012).

Consequently, cheap and high cation exchange performance makes natural zeolite promising in ammonia nitrogen treatment (Huang *et al.* 2015). Moreover, the special framework structure of natural zeolite has a huge pore volume and specific surface area. Lots of adsorption sites can be provided for phosphate, hence it is frequently used to eliminate phosphate in wastewater (Alshameri *et al.* 2014). These functional features make zeolite a potential adsorbent for removing ammonia nitrogen and phosphate from rejected water.

However, the cation exchange capacity of natural zeolite is fairly low. Additionally, the aluminum oxygen tetrahedron in the framework structure is negatively charged, which leads to weak phosphate adsorption capacity because of electrostatic repulsion (Jiang *et al.* 2013; Wen *et al.* 2018). Therefore, natural zeolite needs to be modified to improve its ion exchange and phosphate adsorption capacity. Modification with inorganic salts and metal oxides are extensive and excellent methods to enhance the nitrogen and phosphorus adsorption performance of zeolite (Xu *et al.* 2019). The cations in salt solutions have been used to substitute the alkaline earth metal cations in the zeolite framework (Fu *et al.* 2020), strengthening the NH_4^+ exchange capacity of the zeolite.

Na^+ has a stronger in ion exchange capacity for ammonium compared with various cations, hence a NaCl modification technique has been used to improve the nitrogen removal capacity of zeolite (Fu *et al.* 2020).

Some studies have focused on the loading modification of natural zeolites with metal oxides (Guaya *et al.* 2015; Li *et al.* 2017; Maulana & Takahashi 2018). The unique properties of metal oxides remedy the low phosphate adsorption capacity of natural zeolites. Lanthanum is a rare earth element with high phosphate binding ability and its excellent selectivity has attracted many researchers' attention (Chen *et al.* 2016; Zhang *et al.* 2016a, 2016b, 2016c; Xu *et al.* 2017). In addition, the huge pore volume and specific surface of zeolite provide a number of attachment sites for lanthanum, and lanthanum has shown excellent phosphate adsorption after loading on the zeolite (Xie *et al.* 2014a, 2014b; Pham *et al.* 2019; Song *et al.* 2020).

Zeolite modified with Na and La can achieve better adsorption performance. However, most reported studies used zeolite powder, which made the recovery and reuse of adsorption materials difficult. Moreover, most studies on zeolite concerned the removal of ammonia nitrogen or phosphate individually. There are few investigations into the simultaneous removal of ammonium and phosphate by zeolite. Therefore, it is essential to prepare a recyclable material base on zeolite for the simultaneous removal of ammonia nitrogen and phosphorus from rejected water.

As mentioned above, cheap natural zeolite was selected as the raw material to prepare a composite material (sodium- and lanthanum-modified zeolite particles; Na@La-MZP) for rejected water treatment. The objectives of this study were: (a) to investigate the removal efficiency of Na@La-MZP for ammonia nitrogen and phosphorus, and study the important influencing parameters; (b) to analyze the adsorption characteristics of Na@La-MZP adsorption characteristics by kinetics and isotherms; (c) to study the simultaneous removal mechanism of ammonia nitrogen and phosphorus from rejected water; (d) to evaluate the material's reuse performance, the dynamic treatment capacity of actual wastewater and its economic performance.

MATERIALS AND METHODS

Materials

The natural clinoptilolite used in this study was purchased from Zhejiang Shenshi Mining Co., Ltd (China), and its chemical components are displayed on Table 1. Natural zeolites of 40–60 mesh particle size were used as the original materials. All chemicals in this study, such as NH_4Cl, KH_2PO_4, $LaCl_3{\cdot}6H_2O$, NaCl and C_2H_6O, were analytical grade and obtained from National Pharmaceutical Group Co., Ltd (China). The NH_4^+-N and phosphate content in rejected water from Hubei Township Wastewater Treatment Plant is shown in Table 2. Therefore, simulated wastewater was prepared by dissolving NH_4Cl and KH_2PO_4 for use in this study.

Preparation of Na@La-MZP

The preparation process of Na@La-MZP was as follows (Xu *et al.* 2017): Firstly, 10 g natural zeolite was added to 1.71 mM NaCl solution at a solid-liquid ratio of 1:10 kg/L, and the mixture was shaken at 50 °C for 6 hours. The resulting material was washed multiple times with deionized water until neutral, and dried at 105 °C for 12 hours. Next, 1.25 g $LaCl_3{\cdot}6H_2O$ was dissolved in 50 mL of 20 wt% ethanol solution and stirred for 1 hour. After that, 5 g NaCl-modified zeolite was added to mixture and the pH was adjusted to 11 with 2 M NaOH solution. The mixture reacted in a water bath at 60 °C for 2 hours and then aged in an air-blast drying oven at 80 °C for 12 hours. Next, the zeolite particles were rinsed using deionized water until neutral, and then dried.

Batch adsorption experiments

Batch experiments were carried out to study the simultaneous removal performance of NH_4^+-N and phosphate in rejected water by Na@La-MZP. To determine the appropriate adsorbent dosage, different dosages (2.5–20.0 g/L) of Na@La-MZP were added to the rejected water (NH_4^+-N: 50 mg/L, phosphate: 60 mg/L) at initial pH = 6 and shaken for 12 hours. The effect of initial pH on NH_4^+-N and phosphate adsorption was examined using 1.25 g Na@La-MZP and 100 mL rejected water in the pH range of 2–12, and samples were analyzed at intervals. The pH of the wastewater was adjusted with 0.10 M HCl and NaOH solution. Common anions such as Na^+, Ca^{2+}, K^+, Mg^{2+}, Cl^-, NO_3^-, SO_4^{2-}, HCO_3^- and F^- were evaluated to analyze their effect on the adsorption performance of Na@La-MZP under stable conditions (dosage: 12.50 g/L, initial pH: 6). All the above experiments were performed at

Table 1 | Chemical constituents of natural clinoptilolite

Constituent	SiO_2	Al_2O_3	CaO	Na_2O	K_2O	Fe_2O_3	MgO	Others
Content (%)	69.58	12.20	2.59	2.59	1.13	0.87	0.13	10.91

Table 2 | Characteristics of rejected water

Parameter (unit)	pH	NH_4^+-N (mg/L)	PO_4^{3-} (mg/L)	TN (mg/L)	TP (mg/L)	COD (mg/L)
Value	7.27	48.46	60.51	55.26	63.17	210.85

25 °C with a shaking speed of 160 rpm. At the end of the adsorption period, the supernatant was filtered through a 0.45 μm membrane and the residual concentration in solution was measured by spectrophotometry.

Adsorption kinetics experiments for NH_4^+-N and phosphate were performed. For NH_4^+-N experiments, 1.25 g of Na@La-MZP was added to 100 mL solution with 60 mg/L phosphate and 20–500 mg/L NH_4^+-N. Then the mixtures were stirred at initial pH = 6 and 25 °C, and measured at intervals. The adsorption kinetics of phosphate was similar to NH_4^+-N. Water samples containing 50 mg/L NH_4^+-N and 30–300 mg/L phosphate were prepared. The isothermal adsorption experiments were performed at 25 °C, 35 °C, and 45 °C. The equations and parameters of relevant models are detailed in Text S1 of the Supplementary Information (Chen *et al.* 2013; Xu *et al.* 2019).

The adsorbent-saturated Na@La-MZP was collected to investigate reuse performance. 2 g adsorbent-saturated Na@La-MZP was added to 50 mL 1.0 M NaOH solution, and the mixture was stirred at 25 °C for 2 hours. Then, the supernatant was removed and 50 mL NaOH and Na_2CO_3 mixed solution was added to the original flask and stirred at 50 °C for 2 hours. The desorbed zeolite was washed to neutral with deionized water and dried at 105 °C for 12 hours. The zeolite adsorption-desorption experiment was repeated five times.

Fixed-bed column experiment

A fixed-bed column experiment was carried out in the adsorption column of the up-flow, which was made of a plexiglass column with inner diameter of 4 cm and a height of 30 cm. Coarse-grained quartz sand was arranged between the filter plate and zeolite to prevent adsorbent loss, then 100 g Na@La-MZP was packed into the column. A peristaltic pump was used to control the inlet water flow rate (10 mL/min) and empty bed contact time (12.56 min). The rejected water was applied in the continuous flow systems and analyzed at intervals.

Analytical methods

The concentration of NH_4^+-N and phosphate were determined by Nessler's and molybdenum blue reagent spectrophotometry, respectively. The pH value of the solution was measured with a precision pH meter (STARTER 3100). The concentration of metal cations in solution was determined by inductively coupled plasma-optical emission spectrometry (ICP-OES, PerkinElmer, USA). The specific surface area, pore volume and mesopore distribution of the zeolite were observed using a multi-channel specific surface area and pore size analyzer (TriStar II 3020, USA) at −196.15 °C, and samples were degassed at 200 °C for 4 hours before testing. A field emission scanning electron microscope (SEM, JEM-7500F, Japan) equipped with energy dispersive X-ray spectroscopy (EDS, X-maxN80, Japan) was employed to determine the morphology and elemental composition of zeolite. The crystal structure of the zeolite was recorded by X-ray diffraction (XRD, D8 Advance, Germany). The chemical groups contained in the zeolite were detected by Fourier transform infrared spectrometer (FTIR, Nexus, USA) at room temperature according to the transmission method. The crushed sample and KBr powder were mixed uniformly and compressed into tablets before the FTIR investigation. The surface element types and chemical valences of the zeolite were measured by X-ray photoelectron spectra (XPS, Escalab 250Xi, USA) with monochromatic Al-Kα X-rays as anode. The binding energy (EB) was calibrated using the C 1s peak at 284.8 eV, and XPS Peak 4.1 software was used to perform the peak fitting analysis of O 1s. The surface zero potential (pH_{pzc}) of the zeolite was analyzed by the pH drift method (Sarma & Mahiuddin 2014; Reck *et al.* 2018).

RESULTS AND DISCUSSION

Characterization of Na@La-MZP

The surface morphological characteristics of natural zeolite and Na@La-MZP are shown in Figure 1. The surface of the natural zeolite was rough, with a lot of debris particles (Figure 1(a)), however the Na@La-MZP showed an obvious network structure (Figure 1(b)). Simultaneously, a large number of rod-shaped microcrystals was discovered in its surface, and these crystal structures were similar to $La(OH)_3$ (Dong *et al.* 2017). Compared with natural zeolite, the manufactured Na@La-MZP presented bigger specific surface and pore size (Supplementary Information, Table S1), which was beneficial for NH_4^+-N and phosphate removal (Pham *et al.* 2019). Additionally, the proportion of Na and La element increased from 0.56 to 0.74% and 0.00 to 40.80%, respectively (Figure 1(d)). This observation further confirmed that the adsorption properties of zeolite were enhanced.

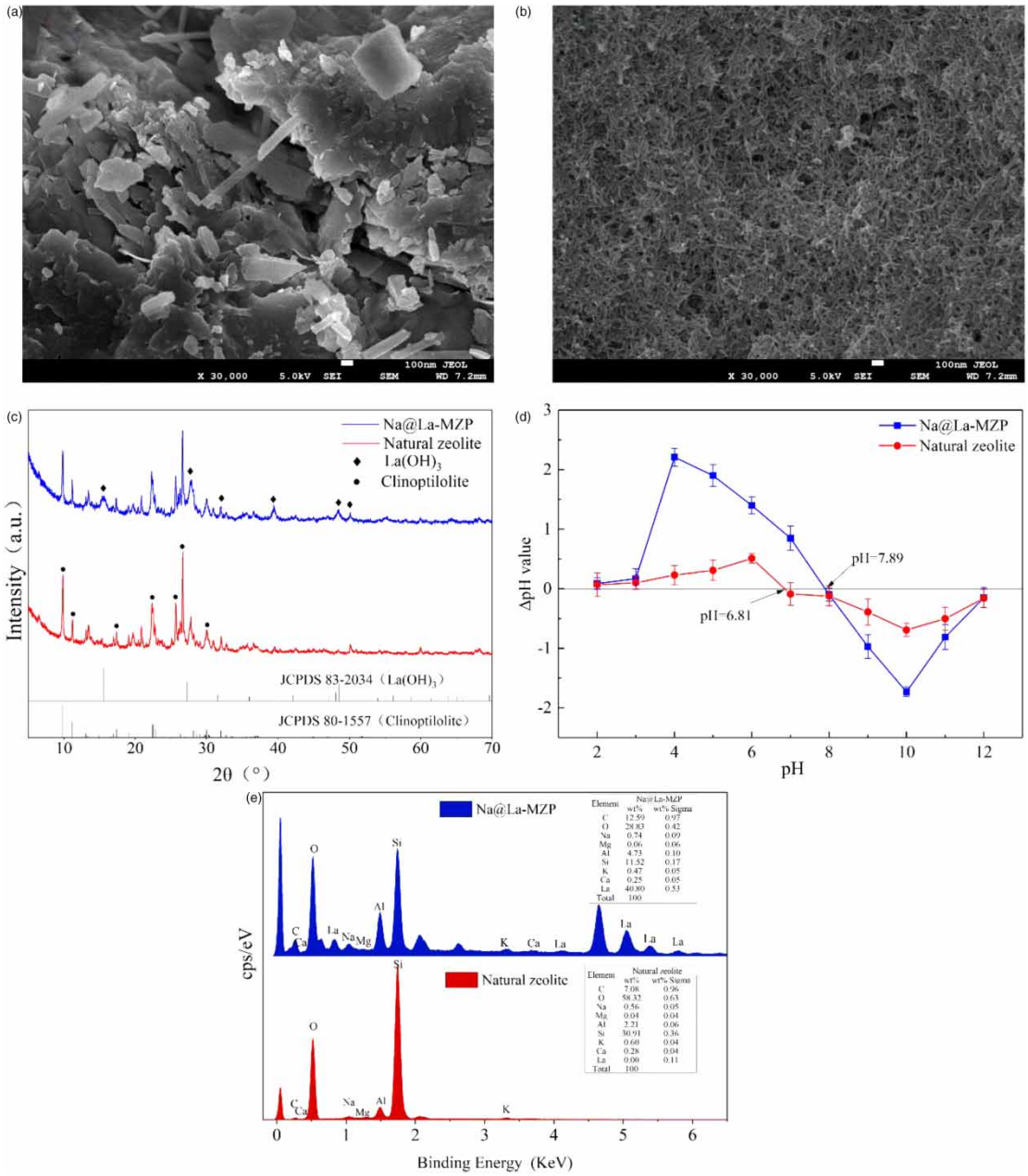

Figure 1 | Characteristics of natural zeolite and Na@La-MZP: (a) and (b) are SEM images of natural zeolite and Na@La-MZP, respectively; (c) XRD patterns; (d) zero point potential (pH_{pzc}); (e) EDS patterns.

The crystal structure of Na@La-MZP is shown in Figure 1(c). The main diffraction peaks of zeolite appeared at 11.22°, 22.45°, 25.67° and 26.65°, which matched the diffraction peaks of clinoptilolite (JCPDS 80-1557). Diffraction peaks of 16.62°, 27.85°, 39.46°, and 48.54° appeared in Na@La-MZP, which proved to be the characteristic peaks of La $(OH)_3$ (JCPDS 83-2034). Therefore, it can be concluded that the lanthanum compound on the zeolite surface was $La(OH)_3$, which was consistent with the SEM results.

Figure 1(d) depicts the pH_{pzc} of natural zeolite and Na@La-MZP. The pH_{zpc} of Na@La-MZP increased from 6.81 to 7.89 compared with natural zeolite. This result could be attributed to the increase in hydroxyl groups on the surface of the zeolite (Yu & Chen 2015). Simultaneously, the high pH_{zpc} implied that the Na@La-MZP was electropositive in a neutral solution, and phosphate adsorption performance was improved by electrostatic attraction.

Simultaneous removal of ammonium and phosphate by Na@La-MZP

Effect of Na@La-MZP dosage

To determine the optimal dosage of Na@La-MZP, the effect of dosage on the simultaneous removal of NH_4^+-N and phosphate was studied. In Figure 2, the removal efficiency of NH_4^+-N and phosphate were improved with the increase of Na@La-MZP dosage. It was observed that the removal efficiency of NH_4^+-N was stable when the dosage reached 7.50 g/L, while the removal efficiency of phosphate increased linearly until the dosage was increased to 12.50 g/L. In addition, it is worth noting that the adsorption amount of per unit mass of zeolite decreased with increasing dosage. This result could be attributed to the fact that available sites were superimposed during adsorbent aggregation (Xie *et al.* 2014a, 2014b). Thus the adsorption efficiency of Na@La-MZP was affected. Considering the economic and removal efficiencies, the adsorbent dosage of Na@La-MZP was selected as 12.50 g/L in subsequent experiments.

Effect of solution initial pH

The solution pH is a critical factor in the adsorption process, because the physico-chemical properties of adsorbent and the type of adsorption are affected by different pH (Liu *et al.* 2013; Xie *et al.* 2014a, 2014b). As shown in Figure 3(a), the Na@La-MZP showed excellent adsorption performance for NH_4^+-N in the pH range of 4–8, and the removal efficiency reached the highest point, 92.61%, at pH 4 after 12 hours. However, the removal efficiency of NH_4^+-N dropped to 69.58 and 20.49% at pH 2 and 12, respectively. These results could be due to the smaller diameter H^+ affecting the ion exchange performance of Na@La-MZP in a strongly acid solution (Vu *et al.* 2017). However, due to the reaction between NH_4^+ and OH^- in a strongly alkaline solution, free NH_3 is formed. NH_3 is a neutral molecule and could not exchange

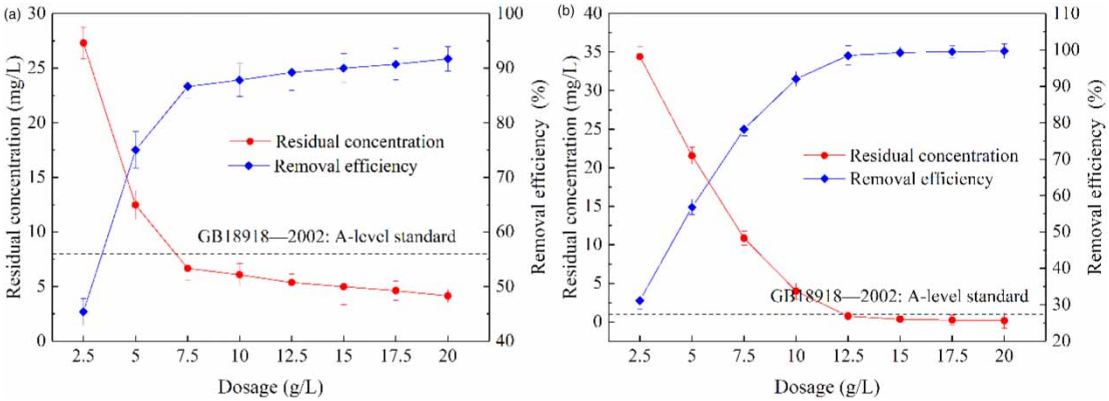

Figure 2 | Effect of Na@La-MZP dosage on the simultaneous removal of NH_4^+-N (a) and phosphate (b).

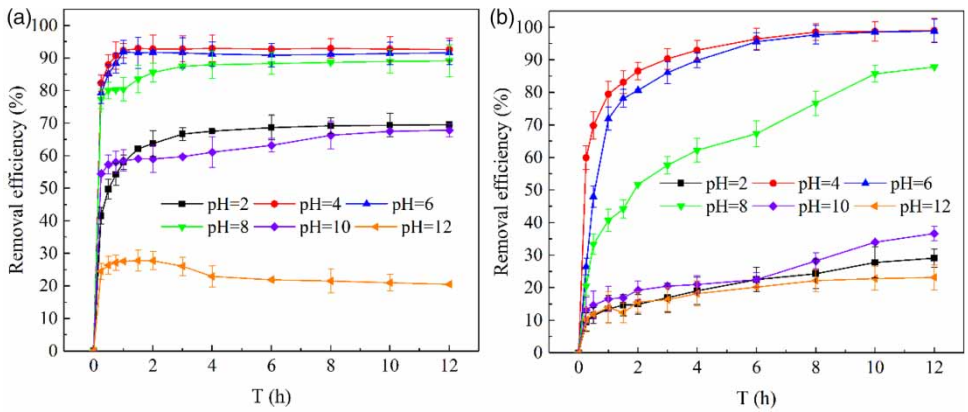

Figure 3 | Effect of initial solution pH on NH_4^+-N (a) and phosphate (b) adsorption capacity of Na@La-MZP.

with metal cations in the Na@La-MZP (Huang *et al.* 2010), so the removal efficiency of NH_4^+-N decreased.

As can be seen from Figure 3(b), Na@La-MZP showed a good phosphate adsorption performance from rejected water in weakly acid conditions (pH = 4–6), and the maximum removal efficiency could reach 99.01%. However, the phosphorus adsorption performance of Na@La-MZP significantly decreased in an acidic or alkaline environment, and the removal efficiency of phosphate declined to 28.08 and 23.15% at pH 2 and 12, respectively. The change of adsorption performance was related to the dissociation reaction of phosphate ions (Supplementary Information, Figure S1) (Zhang *et al.* 2011; Dong *et al.* 2017). The types of phosphate at different solution pH are shown in the following equations:

$$H_3PO_4 \leftrightarrow H_2PO_4^- + H^+ \quad pK_1 = 2.13$$

$$H_2PO_4^- \leftrightarrow HPO_4^{2-} + H^+ \quad pK_2 = 7.20$$

$$HPO_4^{2-} \leftrightarrow PO_4^{3-} + H^+ \quad pK_3 = 12.33$$

The main chemical form of phosphate was $H_2PO_4^-$ in the pH range of 4–6, which made ligand exchange with OH^- on Na@La-MZP easier than the other types. Furthermore, the pH_{zpc} of the modified zeolite was 7.89. The positively charged La-$(OH)^{2+}$ was formed through the deprotonation process of metal active groups on the Na@La-MZP surface (Liu *et al.* 2013), thus the ligand exchange process was promoted and the negatively charged $H_2PO_4^-$ was adsorbed by electrostatic attraction (Dong *et al.* 2017). Lanthanum on the Na@La-MZP surface changed to negatively charged La-O^- in an alkaline environment (Xie *et al.* 2014a, 2014b). In this environment, the electrostatic repulsion between Na@La-MZP and HPO_4^{2-} resulted in the reduction of ligand exchange. Therefore, maintaining the pH at 4–6 could mean a crucial improvement in the simultaneous removal of NH_4^+-N and phosphate in rejected water by Na@La-MZP.

Effect of coexisting ions

The adsorption performance of Na@La-MZP was significantly affected by the various complex ions in rejected water. Therefore, the common metal cations of Na^+, Ca^{2+}, K^+, Mg^{2+} and anions of Cl^-, NO_3^-, SO_4^{2-}, HCO_3^-, F- were selected in this study, and the results are illustrated in Figure 4. The NH_4^+-N adsorption capacity of Na@La-MZP sharply reduced in the presence of K^+. In contrast, the NH_4^+-N adsorption capacity was found to slightly decrease in the presence of Mg^{2+}. This phenomenon was attributed to the exchange sequence and hydration radius of cations. Weatherley & Miladinovic (2004) reported the selective exchange order of zeolite was $K^+ > NH_4^+ > Na^+ > Ca^{2+} > Mg^{2+}$. Furthermore, the K^+ ion has the smallest hydration radius compared to other cations (Rajic *et al.* 2011; Tansel 2012), hence it was easily adsorbed by the Na@La-MZP. This was why the competitive effect of K^+ was greatest for NH_4^+-N removal.

The effect of coexisting anions on the phosphate adsorption performance of Na@La-MZP is shown in Figure 4(b). There was no obvious impact on phosphate adsorption in the presence of SO_4^{2-} and NO_3^-. It is worth noting that the phosphate adsorption rate dropped significantly in the presence of Cl^-, which resulted in a longer adsorption equilibrium time. However, phosphate removal efficiency significantly declined from 99.67 to 92.69% and 72.46% in the presence of HCO_3^- and F^-. The decrease of phosphate adsorption performance resulted in ligand exchange between deprotonated hydroxyl groups on the Na@La-MZP and

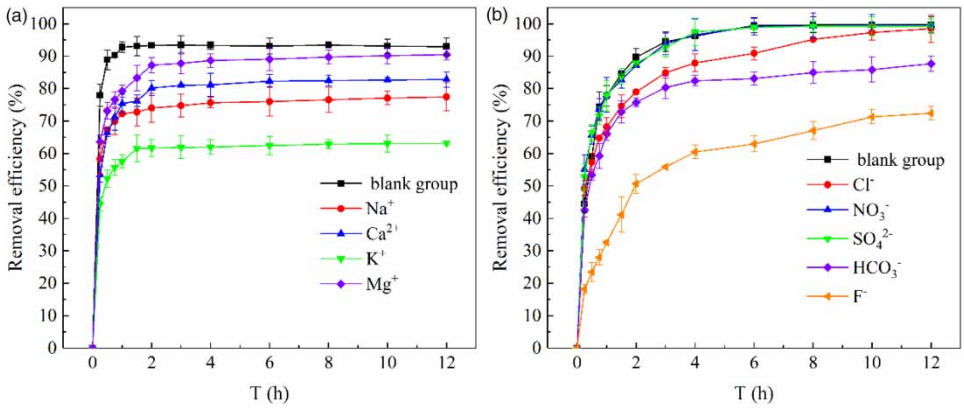

Figure 4 | Effect of coexisting ions on the adsorption capacity of Na@La-MZP for NH_4^+-N (a) and phosphate (b).

coexisting ions (Shi *et al.* 2019). In addition, the affinity of Na@La-MZP to HCO_3^- was higher than PO_4^{3-} because the K_{SP} value of $La_2(CO_3)_3$ (3.98×10^{-34}) was lower than $LaPO_4$ (3.7×10^{-23}) (He *et al.* 2016; Koilraj and Sasaki 2017).

Adsorption kinetics and isotherms

Kinetic analysis was performed to investigate the adsorption of NH_4^+-N and phosphate from rejected water by Na@La-MZP. In Figure S2 (Supplementary Information), NH_4^+-N and phosphate were quickly adsorbed in the early stages, and then reached equilibrium slowly. Simultaneously, the adsorption capacity of Na@La-MZP was improved with the increase in their initial concentrations. The adsorption capacity reached maximum values of 15.83 mg/g and 8.98 mg/g when the initial concentrations of NH_4^+-N and phosphate were increased to 500 and 300 mg/L, respectively. The fitting results of pseudo-first-order, pseudo-second-order dynamic models and correlation parameter of models are shown in Table 3. The correlation coefficients ($R^2 > 0.99$) of the pseudo-second-order kinetics were higher than the pseudo-first-order kinetics for the adsorption of NH_4^+-N and phosphate on Na@La-MZP, and the saturation adsorption amounts were closer to actual data. This result implied that pseudo-second-order dynamic models were more suitable to describe the simultaneous adsorption process of NH_4^+-N and phosphate on Na@La-MZP, which suggested that the adsorption process was controlled by chemical forces (Zhu *et al.* 2012).

The intra-granular diffusion model was applied to clarify the diffusion mechanism of NH_4^+-N and phosphate on Na@La-MZP (Supplementary Information, Figure S3, Table S2). The relation diagram between q_t and $t^{1/2}$ showed that fitting lines of NH_4^+-N and phosphate did not pass through the origin, indicating that the adsorption rate was jointly controlled by liquid film diffusion and particle diffusion (Qiu *et al.* 2017). In addition, the intra-particle diffusion model showed two linear parts, indicating that the adsorption of NH_4^+-N and phosphate was a multistage adsorption processes onto Na@La-MZP (Shi *et al.* 2019). In the first stage, the adsorption sites on the Na@La-MZP surface were quickly occupied by NH_4^+-N and phosphate because of the adsorbent concentration difference and electrostatic attraction. When the surface adsorption sites reached saturation, NH_4^+-N and phosphate diffused into the interior of Na@La-MZP and combined with the interior sites. As the amounts of NH_4^+-N and phosphate in the interior of Na@La-MZP increased, the ion diffusion rate decreased with the increase of diffusion resistance, which was consistent with the fact that the rate constant k_{d1} was obviously larger than k_{d2}. At the same time, the rate constant proved that intragranular diffusion process decided the adsorption rate-control of NH_4^+-N and phosphate (Huang *et al.* 2014).

Adsorption isotherms were used to describe the relationship between the adsorption capacity of the material and the residual concentration in solution (Özer & Dursun 2007). The experimental data were analyzed with Langmuir and Freundlich isotherm adsorption models, and the fitting results are presented in Figure 5 and Table S3 (Supplementary Information). According to the correlation coefficient (R^2), two isothermal adsorption models could fit the adsorption process of Na@La-MZP for NH_4^+-N. But the R^2 value of Langmuir (>0.98) was higher than Freundlich (>0.93); it showed that NH_4^+-N combination sites were evenly distributed on the Na@La-MZP surface and that adsorption was a monolayer adsorption process (Wang *et al.* 2005). The maximum adsorption amount of NH_4^+-N calculated with the

Table 3 | Kinetic adsorption model parameters for NH_4^+-N and phosphate on Na@La-MZP at different concentrations

		Pseudo-first-order kinetics			Pseudo-second-order kinetics		
Concentration (mg/L)		q_e (mg/g)	k_1 (1/min)	R^2	q_e (mg/g)	k_2 (g/mg·min)	R^2
NH_4^+-N	20	1.52	10.905	0.9989	1.52	64.487	0.9999
	50	3.71	7.149	0.9981	3.73	25.765	0.9994
	100	6.76	6.395	0.9958	6.85	5.609	0.9993
	200	10.92	5.356	0.9881	11.28	1.290	0.9997
	300	14.35	5.873	0.9759	15.08	0.681	0.9998
	500	15.29	6.106	0.9785	15.91	0.855	0.9996
Phosphate	30	2.37	4.287	0.9907	2.41	7.431	0.9990
	60	4.64	1.826	0.9799	4.91	0.774	0.9994
	100	6.12	2.519	0.9520	6.69	0.554	0.9993
	150	7.67	3.106	0.9641	8.21	0.637	0.9980
	200	7.77	3.705	0.9556	8.26	0.826	0.9970
	300	8.40	3.136	0.9399	9.10	0.514	0.9970

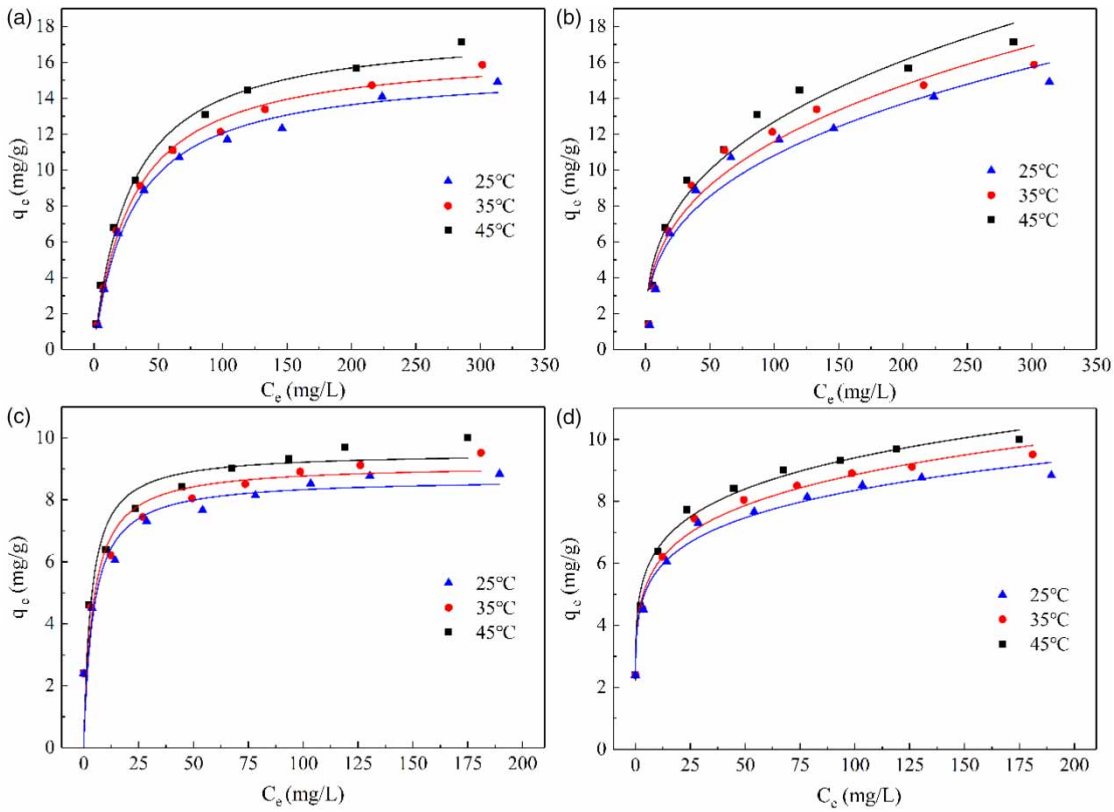

Figure 5 | Isothermal adsorption model of Langmuir (a, c) and Freundlich (b, d) for NH_4^+-N (a, b) and phosphate (c, d) on Na@La-MZP at different temperatures.

Langmuir model was 17.92 mg/g in 45 °C. It is worth noting that the Freundlich ($R^2 > 0.98$) could better describe adsorption behavior of phosphate on Na@La-MZP compared with Langmuir ($R^2 > 0.91$), indicating that phosphate adsorption was a multi-layer chemical adsorption process, and there were different types of chemical reactions on Na@La-MZP surface (Wang *et al.* 2005). In addition, the $1/n$ value in the Freundlich equation is frequently used to describe the adsorbent ability of adsorbents. In this study, values of $1/n$ were less than 0.5, which showed that phosphate was easily adsorbed (Lǔ *et al.* 2013). The maximum adsorption amount of phosphate was 9.53 mg/g. Isotherm analysis showed that the adsorption mechanism of Na@La-MZP for NH_4^+-N and phosphate were significantly different.

Removal mechanism of ammonium and phosphate

The zeolite structure contains many cavities and different size pores. The zeolite framework is negatively charged due to the unbalanced charge of the aluminum oxygen tetrahedron. In order to maintain the charge balance, alkaline earth metal cations are needed to compensate. Common metal cations are Na^+, K^+, Ca^{2+}, and Mg^{2+}. These metal cations are combined with the framework structure through weak bonds in the cavities and pores inside the zeolite. Due to the weak binding force of metal ions with the zeolite framework, it shows great fluidity and ion exchange can occur with NH_4^+ in rejected water. Therefore zeolite could effectively remove ammonia nitrogen. Table S4 (Supplementary Information) displays the concentration and proportion of cations in solution after adsorption equilibrium with the initial NH_4^+-N concentration of 50 mg/L. Clearly, the metal cation content in solution increased significantly in the adsorption equilibrium. This was because the weak binding force within the framework of metal cations in the zeolite and metal cations could be replaced into the solution by the ion exchange reaction with NH_4^+ in rejected water. Specifically, the Na^+ content increased from 0 to 44.39 mg/L and accounted for 89.78% of total cations, which was significantly higher than other metal cations. These results indicated that ion exchange between NH_4^+ and Na^+ on Na@La-MZP was the vital mechanism for NH_4^+-N removal in rejected water. It is worth noting that the total amount of cations in solution after adsorption equilibrium was slightly lower than the NH_4^+ amount on Na@La-MZP, which might be attributed to few NH_4^+ being adsorbed by electrostatic action.

The FTIR spectra of Na@La-MZP before and after adsorption are shown in Figure S4 (Supplementary Information). The absorption peaks near 1,043, 796 and 462 cm^{-1} in the figure are attributed to the unique framework (Si/Al-O tetrahedron) vibration of zeolite. For example, the absorption peak near 1,043 cm^{-1} is Si-O-Si asymmetric tensile vibration, the absorption peak near 796 cm^{-1} is the symmetrical tensile vibration of Si-O-Si or Si-O-Al, and the absorption peak near 462 cm^{-1} is the bending vibration of Si-O or Al-O. In addition to the zeolite skeleton vibration, there are also obvious O-H vibrations such as the O-H stretching vibration in the hydroxyl group near 3,612 and 3,468 cm^{-1} and the O-H bending vibration in the bound water near 1,639 cm^{-1}. A new band at 1,401 cm^{-1} was clearly observed on the adsorbed Na@La-MZP, which was attributed to N-H bending vibration of NH_4^+. Simultaneously, it was observed that the vibration frequency of Si-O-Si or Si-O-Al bands near 796 cm^{-1} was weakened and shifted to low wave number. It was related to the reduction of Na^+ content in the adsorbed Na@La-MZP, so that the spatial structure of material was affected (Król *et al.* 2012; Huang *et al.* 2014).

These results further demonstrated that the removal of NH_4^+-N was related to Na^+ on Na@La-MZP. The bands around 3,612 and 3,468 cm^{-1} were ascribed to the O-H stretching vibration in hydroxyl group (Yu & Chen 2015). The O-H band was significantly weakened after adsorption, which could be attributed to the ligand exchange between hydroxyl groups in the Na@La-MZP and phosphate. In addition, the band initially at 1,043 cm^{-1} shifted to 1,047 cm^{-1} and the vibration frequency was strengthened, which was assigned to the asymmetric tensile vibration of P-O (Li *et al.* 2009). At the same time, the band vibration frequency at 611 cm^{-1} was significantly enhanced due to the bending vibration of O-P-O (Liu *et al.* 2013). Therefore, Na@La-MZP surface inner-sphere complexes were formed by ligand interaction.

The XPS characterization of material was used to further explore the removal mechanism of NH_4^+-N and phosphate by Na@La-MZP (Figure 6). A new peak of P 2p (132.34 eV) clearly appeared after adsorption (Figure 6(c)), and the N 1s (401.31 eV) peak was also enhanced (Figure 6(b)). These phenomena indicated that P and N were successfully adsorbed by Na@La-MZP. In detail, the binding energy of P 2p XPS spectrum was reduced by 1.66 eV compared with the standard P 2p (134.00 eV) of pure KH_2PO_4 (Zhang *et al.* 2016a, 2016b, 2016c), which confirmed the formation of new phosphate complexes on Na@La-MZP (Acelas *et al.* 2015; Wu *et al.* 2019). Two sets peaks of La 3d in the XPS spectrum were observed (Figure 6(e)). $E_B[La\ 3d_{5/2}] =$ 834.38 eV and 838.08 eV and $E_B[La\ 3d_{3/2}] = 851.28$ eV and 854.88 eV before adsorption were consistent with the binding energy of $La(OH)_3$ (Sunding *et al.* 2011). The peak values of La $3d_{5/2}$ (834.88 eV and 838.28 eV) and La $3d_{3/2}$ (851.38 eV and 855.18 eV) moved in the direction of high binding energy. In addition, Δ (La $3d_{5/2}$) decreased from 3.70 eV to 3.40 eV while Δ (La $3d_{3/2}$) increased from 3.60 eV to 3.80 eV, which indicated that La-OP inner-sphere complexes were formed under strong interaction force on Na@La-MZP (Fang *et al.* 2018; Hao *et al.* 2019).

According to the different binding energy of different oxides, O 1s spectrum of Na@La-MZP was separated into three types: bound water (H_2O) corresponds to 532.09 eV, metal-bound hydroxyl (M-OH) corresponds to 531.07 eV and metal oxides (M-O) correspond to 530.11 eV (Figure 6(f)) (Islam *et al.* 2014; Yu & Chen 2015). The detailed analysis of O 1s before and after adsorption is summarized in Table S5 (Supplementary Information). Note that the relative content of M-OH in Na@La-MZP decreased from 60.05 to 49.42%, while M-O increased from 26.96 to 35.61%. These results indicated ligand exchange of O-H with O-P, and inner-sphere complex formation in La-O-P (Yu & Chen 2015; Zhang *et al.* 2016a, 2016b, 2016c; Shi *et al.* 2019).

In summary, the effective removal mechanism of NH_4^+-N could be attributed to ion exchange with Na^+ in Na@La-MZP, and the removal mechanisms of phosphate were electrostatic adsorption, formation of La-O-P inner-sphere complexes and ligand exchange of hydroxyl groups.

Recycling performance of Na@La-MZP

Recycling performance is an important index to evaluate the performance of adsorbents. The NH_4^+-N and phosphate in the saturated modified zeolite were regenerated successively by two-step desorption. From Figure S5a (Supplementary Information), NaOH solution showed good desorption capacity for NH_4^+-N compared with phosphate. The NH_4^+-N desorption efficiency could reach 93.89% while phosphate was only 4.40% in 1.0 M NaOH solution. This difference in desorption might be attributed to the ion exchange reaction between Na^+ and NH_4^+ on the modified zeolite and PO_4^{3-} being less affected by NaOH. Therefore, NaOH-Na_2CO_3 mixed solution was used as regenerators in the second step of desorption to further improve the phosphate desorption efficiency of Na@La-MZP. The desorption efficiency is shown in Figure S5 (Supplementary Information).

The phosphate desorption rate gradually increased with the rise of NaOH concentration at a fixed molar ratio of

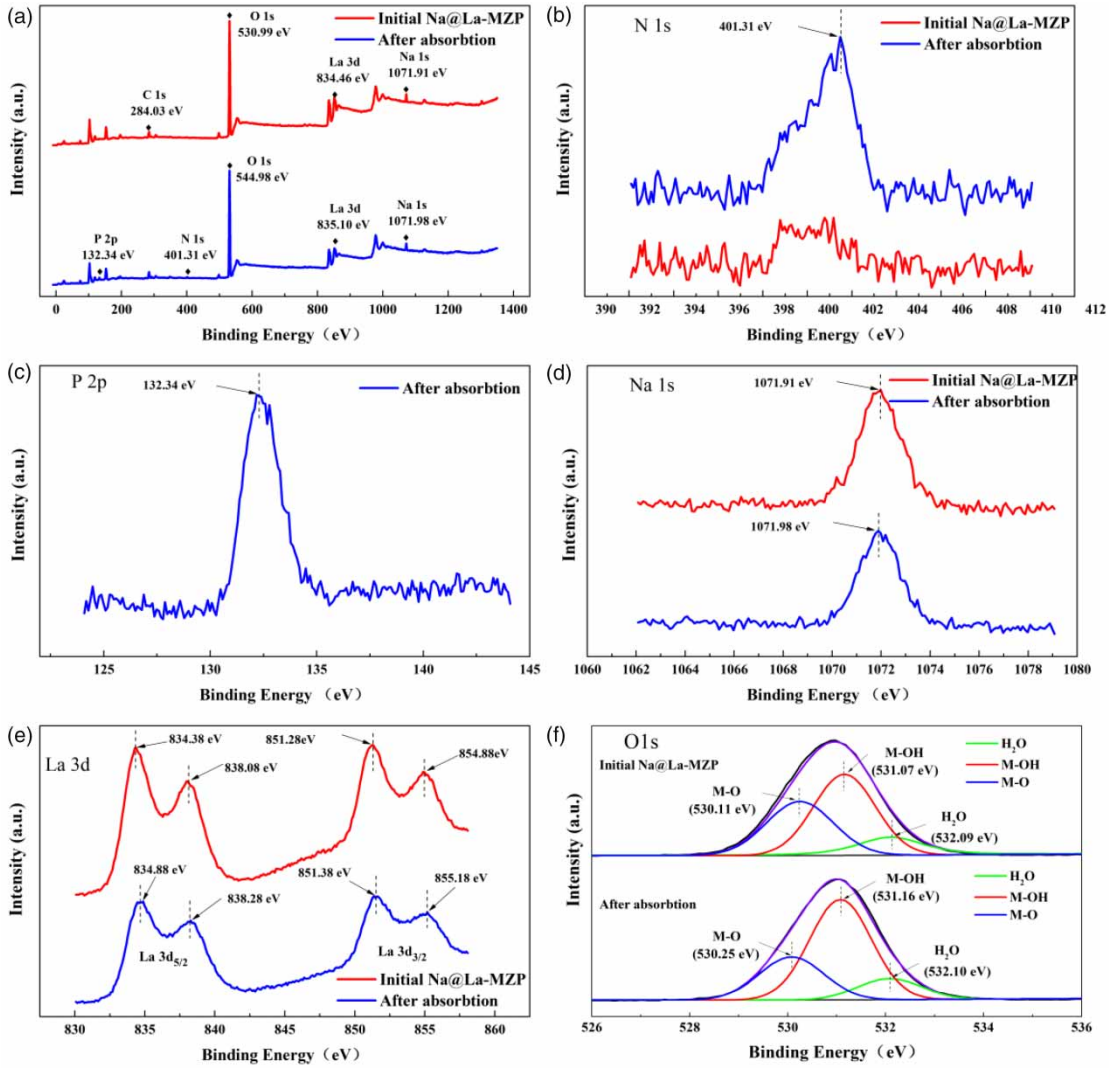

Figure 6 | XPS spectrum of Na@La-MZP before and after adsorption.

NaOH and Na_2CO_3, while the NH_4^+-N desorption efficiency remained at about 4.00%. The phosphate desorption efficiency reached a maximum of 66.47% with 3 M NaOH mixed with 3 M $NaCO_3$. Thus, the concentration of NaOH and Na_2CO_3 mixed solution was selected as the desorption agent to perform the second step of the regeneration of saturated Na@La-MZP.

Adsorption-desorption cycle regeneration experiments were performed five times to evaluate the reusability of Na@La-MZP (Figure 7). Overall, the adsorption performance of Na@La-MZP decreased gradually with the increase of the regeneration times. The removal efficiency of NH_4^+-N and phosphate decreased significantly, and it decreased from 91.84 and 98.84% to 81.42 and 85.72% in second adsorption, respectively. After five cycles of

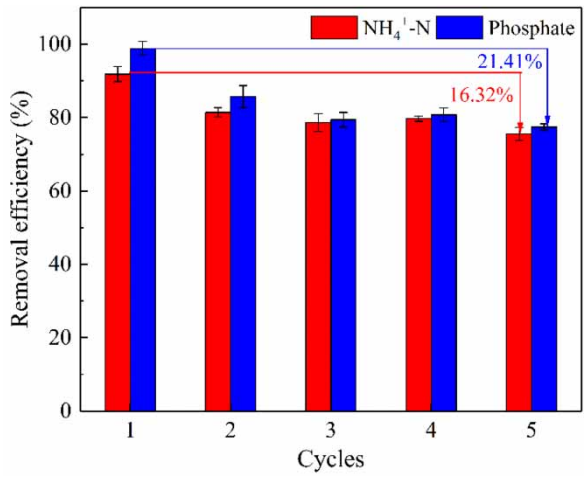

Figure 7 | Recycling performance of Na@La-MZP.

adsorption-desorption, the removal rates of NH_4^+-N and phosphate decreased by 16.32 and 21.41%, respectively, compared with the initial Na@La-MZP. This phenomenon of adsorption capacity reduction was attributed to the leaching of Na/La compounds and presence of some irreversible adsorption sites such as chemical adsorption sites of phosphate. Nevertheless, the removal rate of NH_4^+-N and phosphate could remain above 75% after five cycles, which indicated that Na@La-MZP could be reused in rejected water treatment.

Fixed-bed application of Na@La-MZP in actual rejected water

In order to prove the practical application potential of Na@La-MZP, a fixed-bed adsorption experiment was carried out with the rejected water of Hubei Township Sewage Treatment Plant. The water quality parameters of wastewater are listed in Table 2. The removal efficiency of Na@La-MZP with NH_4^+-N and phosphate in actual wastewater was slightly lower than that in simulated wastewater (Figure S6, Supplementary Information). In particular, the breakthrough time of NH_4^+-N and phosphate in actual wastewater was reduced by 3.11 hours and 4.53 hours, respectively. This was because there are various competitive ions and organic pollutants in actual wastewater alongside the target pollutants. These substances will occupy the active adsorption sites on the surface of the adsorbent, thereby influencing the adsorption performance of the material. Nevertheless, Na@La-MZP still showed excellent treatment capacity for actual wastewater from the perspective of actual treatment effect, which indicated that Na@La-MZP could be used as a potential adsorbent to simultaneously remove NH_4^+-N and phosphorus from rejected water.

Economic evaluation

Na@La-MZP after adsorption can be used in agriculture and as a raw material in fertilizers because these zeolite solids are loaded in nitrogen and phosphorus (Markou *et al.* 2014). In addition, its selling price can justify the expense of zeolite consumed during the process of adsorption. The cost of the process was mostly due to the brine used for the modification of the zeolite. Thus, ignoring the staffing and energy costs, an estimated cost for treating 1 L rejected water is dependent on the cost of 8.84 mM $LaCl_3{\cdot}6H_2O$ (market price 0.074 US$/kg). Consequently, the treatment cost of the proposed process can be calculated to be 0.22 US$/$m^3$ rejected water.

CONCLUSIONS

In this study, a new type of Na@La-MZP adsorbent was successfully fabricated and used to simultaneously remove NH_4^+-N and phosphorus from rejected water. Na@La-MZP could remove 92.61% ammonia nitrogen (50 mg/L) and 99.01% phosphate (60 mg/L) at the optimal conditions of dosage 12.5 g/L, initial pH 6.0 and reaction time 12 hours, which made the effluent satisfy the discharge standard (GB 18918-2002) for municipal WWTPs in China. The Na@La-MZP exhibited excellent adsorption performance for NH_4^+-N and phosphorus at pH 4–6.

Coexisting cations inhibited the removal of ammonium in the order $K^+ > Na^+ > Ca^{2+} > Mg^{2+}$, and anions affected the adsorption of phosphate in the order $F^- > HCO_3^- > Cl^- > SO_4^{2-} > NO_3^-$. Pseudo-second-order kinetics could well describe the adsorption process, and the adsorption rate was mainly controlled by the intra-particle diffusion process. The effective removal mechanism of NH_4^+-N could be attributed to ion exchange with Na^+ in Na@La-MZP and the removal mechanisms of phosphate were electrostatic adsorption, formation of La-O-P inner-sphere complexes and ligand exchange of hydroxyl groups.

The results of reuse and actual wastewater treatment experiments implied that Na@La-MZP as an adsorbent could simultaneously and efficiently remove NH_4^+-N and phosphate. Research into inexpensive modification technology will be a vital development direction in the future. We suggest strengthening the research on the regeneration of zeolite, which would help to enlarge the utilization period of zeolite. The development of economical synthetic zeolite is an essential research direction for achieving the sustainable utilization of zeolite.

ACKNOWLEDGEMENT

This work was supported by National Natural Science Foundation of China project 51108360 and 51208397, Science and Technology Infrastructure Program in Hubei (Grant No.2015BCA304).

DATA AVAILABILITY STATEMENT

All relevant data are included in the paper or its Supplementary Information.

REFERENCES

Acelas, N., Martin, B., López, D. & Jefferson, B. 2015 Selective removal of phosphate from wastewater using hydrated metal oxides dispersed within anionic exchange media. *Chemosphere* **119**, 1353–1360.

Alshameri, A., Yan, C. & Lei, X. 2014 Enhancement of phosphate removal from water by TiO_2/Yemeni natural zeolite: preparation, characterization and thermodynamic. *Microporous and Mesoporous Materials* **196**, 145–157.

Chen, Z., Wang, T., Jin, X., Chen, Z., Megharaj, M. & Naidu, R. 2013 Multifunctional kaolinite-supported nanoscale zero-valent iron used for the adsorption and degradation of crystal violet in aqueous solution. *Journal of Colloid and Interface Science* **398**, 59–66.

Chen, M., Huo, C., Li, Y. & Wang, J. 2016 Selective adsorption and efficient removal of phosphate from aqueous medium with graphene-lanthanum composite. *ACS Sustainable Chemistry & Engineering* **4**, 1296–1302.

Cheng, H., Stabnikov, V. & Ivanov, V. 2010 The removal of nitrogen and phosphorus from reject water of municipal wastewater treatment plant using ferric and nitrate bioreductions. *Bioresource Technology* **101**, 3992–3999.

Copetti, D., Finsterle, K., Marziali, L., Stefani, F., Tartari, G., Douglas, G., Reitzel, K., Spears, B., Winfield, I., Crosa, G., D'Haese, P., Yasseri, S. & Lurling, M. 2016 Eutrophication management in surface waters using lanthanum modified bentonite: a review. *Water Research* **97**, 162–174.

Dong, S., Wang, Y., Zhao, Y., Zhou, X. & Zheng, H. 2017 La^{3+}/$La(OH)_3$ loaded magnetic cationic hydrogel composites for phosphate removal: effect of lanthanum species and mechanistic study. *Water Research* **126**, 433–441.

Fang, L., Liu, R., Li, J., Xu, C., Huang, L. & Wang, D. 2018 Magnetite/lanthanum hydroxide for phosphate sequestration and recovery from lake and the attenuation effects of sediment particles. *Water Research* **130**, 243–254.

Fu, H., Li, Y., Yu, Z., Shen, J., Li, J., Zhang, M., Ding, T., Xu, L. & Lee, S. 2020 Ammonium removal using a calcined natural zeolite modified with sodium nitrate. *Journal of Hazardous Materials* **393**, 122481.

Ge, D., Yuan, H., Shen, Y., Zhang, W. & Zhu, N. 2019 Improved sludge dewaterability by tannic acid conditioning: temperature, thermodynamics and mechanism studies. *Chemosphere* **230**, 14–23.

Guaya, D., Valderrama, C., Farran, A., Armijos, C. & Cortina, J. 2015 Simultaneous phosphate and ammonium removal from aqueous solution by a hydrated aluminum oxide modified natural zeolite. *Chemical Engineering Journal* **271**, 204–213.

Hao, H., Wang, Y. & Shi, B. 2019 $NaLa(CO_3)_2$ hybridized with Fe_3O_4 for efficient phosphate removal: synthesis and adsorption mechanistic study. *Water Research* **155**, 1–11.

He, Y., Lin, H., Dong, Y., Liu, Q. & Wang, L. 2016 Simultaneous removal of ammonium and phosphate by alkaline-activated and lanthanum-impregnated zeolite. *Chemosphere* **164**, 387–395.

Hu, D., Zhou, Z., Shen, X., Wei, H., Jiang, L. & Lv, Y. 2015 Effects of alkalinity on membrane bioreactors for reject water treatment: performance improvement, fouling mitigation and microbial structures. *Bioresource Technology* **197**, 217–226.

Huang, H., Xiao, X., Yan, B. & Yang, L. 2010 Ammonium removal from aqueous solutions by using natural Chinese (Chende) zeolite as adsorbent. *Journal of Hazardous Materials* **175**, 247–252.

Huang, W., Li, D., Liu, Z., Tao, Q., Zhu, Y., Yang, J. & Zhang, Y. 2014 Kinetics, isotherm, thermodynamic, and adsorption mechanism studies of $La(OH)_3$-modified exfoliated vermiculites as highly efficient phosphate adsorbents. *Chemical Engineering Journal* **236**, 191–201.

Huang, H., Yang, L., Xue, Q., Liu, J., Hou, L. & Ding, L. 2015 Removal of ammonium from swine wastewater by zeolite combined with chlorination for regeneration. *Journal of Environmental Management* **160**, 333–341.

Iqbal, J., Shah, N., Sayed, M., Imran, M., Muhammad, N., Howari, F., Alkhoori, A., Khan, J., Khan, Z., Bhatnagr, A., Polychronopoulou, K., Ismail, I. & Haija, M. 2019 Synergistic effects of activated carbon and nano-zerovalent copper on the performance of hydroxyapatite-alginate beads for the removal of As^{3+} from aqueous solution. *Journal of Cleaner Production* **235**, 875–886.

Iqbal, J., Shah, N., Sayed, M., Niazi, N., Imran, M., Khan, J., Khan, Z., Hussien, A., Polychronopoulou, K. & Howari, F. 2021 Nano-zerovalent manganese/biochar composite for the adsorptive and oxidative removal of Congo-red dye from aqueous solutions. *Journal of Hazardous Materials* **403**, 123854.

Islam, M., Mishra, S., Swain, S., Patel, R., Dey, R. & Naushad, M. 2014 Evaluation of phosphate removal efficiency from aqueous solution by polypyrrole/BOF slag nanocomposite. *Separation Science and Technology* **49**, 2668–2680.

Ivanov, V., Kuang, S., Stabnikov, V. & Guo, C. 2009 The removal of phosphorus from reject water in a municipal wastewater treatment plant using iron ore. *Journal of Chemical Technology & Biotechnology* **84**, 78–82.

Jiang, C., Jia, L., He, Y., Zhang, B., Kirumba, G. & Xie, J. 2013 Adsorptive removal of phosphorus from aqueous solution using sponge iron and zeolite. *Journal of Colloid and Interface Science* **402**, 246–252.

Jiang, N., Shang, R., Heijman, S. & Rietveld, L. 2018 High-silica zeolites for adsorption of organic micro-pollutants in water treatment: a review. *Water Research* **144**, 145–161.

Koilraj, P. & Sasaki, K. 2017 Selective removal of phosphate using La-porous carbon composites from aqueous solutions: batch and column studies. *Chemical Engineering Journal* **317**, 1059–1068.

Król, M., Mozgawa, W., Jastrzębski, W. & Barczyk, K. 2012 Application of IR spectra in the studies of zeolites from D4R and D6R structural groups. *Microporous and Mesoporous Materials* **156**, 181–188.

Kumari, A., Kumar, A., Sharma, G., Iqbal, J., Naushad, M. & Stadler, F. 2020 Constructing Z-scheme LaTiO2N/g-C3N4@Fe3O4 magnetic nano heterojunctions with promoted charge separation for visible and solar removal of indomethacin. *Journal of Water Process Engineering* **36**, 101391.

Li, H., Ru, J., Yin, W., Liu, X., Wang, J. & Zhang, W. 2009 Removal of phosphate from polluted water by lanthanum doped vesuvianite. *Journal of Hazardous Materials* **168**, 326–330.

Li, Y., Fan, Y., Li, X. & Wu, D. 2017 Evaluation of zeolite/hydrous aluminum oxide as a sediment capping agent to reduce nutrients level in a pond. *Ecological Engineering* **101**, 170–178.

Liu, J., Zhou, Q., Chen, J., Zhang, L. & Chang, N. 2013 Phosphate adsorption on hydroxyl–iron–lanthanum doped activated carbon fiber. *Chemical Engineering Journal* **215–216**, 859–867.

Lǔ, J., Liu, H., Liu, R., Zhao, X., Sun, L. & Qu, J. 2013 Adsorptive removal of phosphate by a nanostructured Fe–Al–Mn trimetal oxide adsorbent. *Powder Technology* **233**, 146–154.

Markou, G., Vandamme, D. & Muylaert, F. 2014 Using natural zeolite for ammonia sorption from wastewater and as nitrogen releaser for the cultivation of *Arthrospira platensis*. *Bioresource Technology* **155**, 373–378.

Maulana, I. & Takahashi, F. 2018 Cyanide removal study by raw and iron-modified synthetic zeolites in batch adsorption experiments. *Journal of Water Process Engineering* **22**, 80–86.

Mazloomi, F. & Jalali, M. 2016 Ammonium removal from aqueous solutions by natural Iranian zeolite in the presence of organic acids, cations and anions. *Journal of Environmental Chemical Engineering* **4**, 1664–1673.

Montalvo, S., Guerrero, L., Borja, R., Sánchez, E., Milán, Z., Cortés, I. & Angeles de la la Rubia, M. 2012 Application of natural zeolites in anaerobic digestion processes: a review. *Applied Clay Science* **58**, 125–133.

Motsi, T., Rowson, N. & Simmons, M. 2009 Adsorption of heavy metals from acid mine drainage by natural zeolite. *International Journal of Mineral Processing* **92**, 42–48.

Özer, A. & Dursun, G. 2007 Removal of methylene blue from aqueous solution by dehydrated wheat bran carbon. *Journal of Hazardous Materials* **146**, 262–269.

Pham, T., Lee, K., Kim, M., Seo, J. & Lee, C. 2019 La-modified ZSM-5 zeolite beads for enhancement in removal and recovery of phosphate. *Microporous and Mesoporous Materials* **279**, 37–44.

Qiu, H., Liang, C., Yu, J., Zhang, Q., Song, M. & Chen, F. 2017 Preferable phosphate sequestration by nano-La(III) (hydr) oxides modified wheat straw with excellent properties in regeneration. *Chemical Engineering Journal* **315**, 345–354.

Rajic, N., Stojakovic, D., Daneu, N. & Recnik, A. 2011 The formation of oxide nanoparticles on the surface of natural clinoptilolite. *Journal of Physics and Chemistry of Solids* **72**, 800–803.

Reck, I., Paixao, R., Bergamasco, R., Vieira, M. & Salcedo Vieira, A. 2018 Removal of tartrazine from aqueous solutions using adsorbents based on activated carbon and *Moringa oleifera* seeds. *Journal of Cleaner Production* **171**, 85–97.

Ren, W., Zhou, Z., Jiang, L., Hu, D., Qiu, Z., Wei, H. & Wang, L. 2015 A cost-effective method for the treatment of reject water from sludge dewatering process using supernatant from sludge lime stabilization. *Separation and Purification Technology* **142**, 123–128.

Sarma, J. & Mahiuddin, S. 2014 Specific ion effect on the point of zero charge of α-alumina and on the adsorption of 3,4-dihydroxybenzoic acid onto α-alumina surface. *Colloids and Surfaces A: Physicochemical and Engineering Aspects* **457**, 419–424.

Shi, W., Fu, Y., Jiang, W., Ye, Y., Kang, J., Liu, D., Ren, Y., Li, D., Luo, C. & Xu, Z. 2019 Enhanced phosphate removal by zeolite loaded with Mg-Al-La ternary (hydr)oxides from aqueous solutions: performance and mechanism. *Chemical Engineering Journal* **357**, 33–44.

Song, Q., Huang, S., Xu, L., Wang, N., Hu, Z., Luo, X. & Zheng, Z. 2020 Synthesis of magnetite/lanthanum hydroxide composite and magnetite/aluminum hydroxide composite for removal of phosphate. *Science of the Total Environment* **723**, 137838.

Sunding, M., Hadidi, K., Diplas, S., Løvvik, O., Norby, T. & Gunnæs, A. 2011 XPS characterisation of in situ treated lanthanum oxide and hydroxide using tailored charge referencing and peak fitting procedures. *Journal of Electron Spectroscopy and Related Phenomena* **184**, 399–409.

Tansel, B. 2012 Significance of thermodynamic and physical characteristics on permeation of ions during membrane separation: hydrated radius, hydration free energy and viscous effects. *Separation and Purification Technology* **86**, 119–126.

Torà, J., Lafuente, J., Belinchón, C., Bouchy, L., Carrera, J. & Baeza, J. 2014 High-throughput nitritation of reject water with a novel ammonium control loop: stable effluent generation for anammox or heterotrophic denitritation. *Chemical Engineering Journal* **243**, 265–271.

Vu, T., Trinh, V., Doan, D., Van, H., Nguyen, T., Vigneswaran, S. & Ngo, H. 2017 Removing ammonium from water using modified corncob-biochar. *Science of the Total Environment* **579**, 612–619.

Wang, S., Boyjoo, Y., Choueib, A. & Zhu, Z. 2005 Removal of dyes from aqueous solution using fly ash and red mud. *Water Research* **39**, 129–138.

Weatherley, L. & Miladinovic, N. 2004 Comparison of the ion exchange uptake of ammonium ion onto New Zealand clinoptilolite and mordenite. *Water Research* **38**, 4305–4312.

Wen, J., Dong, H. & Zeng, G. 2018 Application of zeolite in removing salinity/sodicity from wastewater: a review of mechanisms, challenges and opportunities. *Journal of Cleaner Production* **197**, 1435–1446.

Wu, Y., Li, X., Yang, Q., Wang, D., Xu, Q., Yao, F., Chen, F., Tao, Z. & Huang, X. 2019 Hydrated lanthanum oxide-modified diatomite as highly efficient adsorbent for low-concentration phosphate removal from secondary effluents. *Journal of Environmental Management* **231**, 370–379.

Xie, J., Wang, Z., Fang, D., Li, C. & Wu, D. 2014a Green synthesis of a novel hybrid sorbent of zeolite/lanthanum hydroxide and its application in the removal and recovery of phosphate from water. *Journal of Colloid and Interface Science* **423**, 13–19.

Xie, J., Wang, Z., Lu, S., Wu, D., Zhang, Z. & Kong, H. 2014b Removal and recovery of phosphate from water by lanthanum hydroxide materials. *Chemical Engineering Journal* **254**, 163–170.

Xu, R., Zhang, M., Mortimer, R. & Pan, G. 2017 Enhanced phosphorus locking by novel lanthanum/aluminum–hydroxide composite: implications for eutrophication control. *Environmental Science & Technology* **51**, 3418–3425.

Xu, K., Lin, F., Dou, X., Zheng, M., Tan, W. & Wang, C. 2018 Recovery of ammonium and phosphate from urine as value-added fertilizer using wood waste biochar loaded with magnesium oxides. *Journal of Cleaner Production* **187**, 205–214.

Xu, Q., Li, W., Ma, L., Cao, D., Owens, G. & Chen, Z. 2019 Simultaneous removal of ammonia and phosphate using green synthesized iron oxide nanoparticles dispersed onto zeolite. *Science of the Total Environment* **703**, 135002.

Yu, Y. & Chen, J. P. 2015 Key factors for optimum performance in phosphate removal from contaminated water by a Fe–Mg–La tri-metal composite sorbent. *Journal of Colloid and Interface Science* **445**, 303–311.

Zhang, J., Shen, Z., Shan, W., Mei, Z. & Wang, W. 2011 Adsorption behavior of phosphate on lanthanum(III)-coordinated diamino-functionalized 3D hybrid mesoporous silicates material. *Journal of Hazardous Materials* **186**, 76–83.

Zhang, H., Li, A., Zhang, W. & Shuang, C. 2016a Combination of Na-modified zeolite and anion exchange resin for advanced treatment of a high ammonia-nitrogen content municipal effluent. *Journal of Colloid and Interface Science* **468**, 128–135.

Zhang, Y., Pan, B., Shan, C. & Gao, X. 2016b Enhanced phosphate removal by nanosized hydrated La(III) oxide confined in cross-linked polystyrene networks. *Environmental Science & Technology* **50**, 1447–1454.

Zhang, Q., Teng, J., Zou, G., Peng, Q., Du, Q., Jiao, T. & Xiang, J. 2016c Efficient phosphate sequestration for water purification by unique sandwich-like MXene/Magnetic iron oxide nanocomposites. *Nanoscale* **8**, 7085–7093.

Zhu, K., Fu, H., Zhang, J., Lv, X., Tang, J. & Xu, X. 2012 Studies on removal of NH_4^+-N from aqueous solution by using the activated carbons derived from rice husk. *Biomass and Bioenergy* **43**, 18–25.

First received 2 September 2020; accepted in revised form 28 October 2020. Available online 6 November 2020